https://doi.org/10.5194/egusphere-2026-795
Preprint. Discussion started: 17 February 2026

Energetically Stringent Quantification of Water Vapor Supersaturation at Cloud Base

Ramon C. Braga[1], Daniel Harrison[1], Manfred Wendisch[2] and Rachel Albrecht[3]

[1] Reefs and Oceans Research Cluster, National Marine Science Centre, Southern Cross University, Coffs Harbour, Australia.
[2] Leipzig Institute for Meteorology, Leipzig University, Leipzig, Germany.
[3] Instituto de Astronomia, Geofísica e Ciências Atmosféricas, Universidade de São Paulo, São Paulo, Brazil.

Correspondence to: Ramon C. Braga (ramon.braga@scu.edu.au)

Abstract. We quantify water vapor supersaturation (S_v) at warm cloud base by describing the ascent of a saturated (cloudy) air parcel as a reversible cloud-adiabatic process. In this framework, the parcel's isobaric enthalpy is conserved along the ascent. The latent heat release (Q) during condensational growth of cloud condensation nuclei (CCN) and droplets is internally redistributed according to the first law of thermodynamics, such that the energy balance is partitioned between the parcel's internal energy (U) and the saturation work of water vapor (W_s). We find that the fraction of Q associated with ΔU and W_s corresponds to liquid-phase supersaturation (S_l) and S_v, respectively. Closure analyses of airborne measurements at cloud bases of growing cumuli over the Amazon Basin demonstrate that the droplet number concentration N_d scales with S_v and agrees within the uncertainty range with the CCN(S_v) activation spectra measured below cloud base. The new methodology allows the calculation of $N_d(S_v)$ spectra from airborne measurements at cloud bases. Our results suggest that adiabatic models assuming full conversion of phase-change energy into condensational growth tend to overestimate the liquid water content. During the cloud parcel ascent, a finite fraction of this energy is expended as vapor expansion work, reducing the amount available for vapor-to-liquid conversion. Neglecting this energetic partition leads to an overestimation of the latent heat released during condensational growth of particles, cloud parcel buoyancy and vertical acceleration.

1 Introduction

Understanding cloud formation processes and their impact on the atmospheric energy budget and water cycle is crucial for numerical weather and climate models (IPCC, 2021). Liquid water cloud droplets form in a rising humid air parcel, which expands due to decreasing air pressure and as a result cools during ascent until supersaturation with respect to liquid water is reached. Subsequently, the water vapor condenses onto surfaces provided by a subset of the preexisting aerosol particles that act as cloud condensation nuclei (CCN). The condensation of water vapor on aerosol particles and the subsequent activation and growth of cloud droplets are described by the Köhler theory (Köhler, 1936). Despite extensive field observations and

https://doi.org/10.5194/egusphere-2026-795
Preprint. Discussion started: 17 February 2026

numerical modeling based on Köhler theory, the water-vapor supersaturation (S_v) at cloud base remains an inferred quantity restricted by certain assumptions and lacking a thermodynamically constrained foundation that could be validated by in-situ measurements (Korolev and Mazin, 2003; Pinsky et al., 2012; Prabhakaran et al., 2020).

Modeling and observational studies have been performed in various parts of the world to improve our understanding of the relationship between aerosol properties and their ability to form cloud droplets as a function of S_v (Ervens et al., 2010; Rissler et al., 2004; Wang et al., 2008). These studies compare the predicted number concentration of CCN according to Köhler theory based on particle size and composition to results from CCN counting instruments at different S_v. Similar analyses were performed from measurements of CCN(S_v) spectra below cloud bases and parametrizations of the number concentration of droplets (N_d) as a function S_v in clouds (Campos Braga et al., 2017). Furthermore, N_d at cloud bases is commonly calculated in adiabatic cloud models based on the hygroscopic growth of CCN particles within a rising humid air parcel with a prescribed hygroscopicity of the CCN particles and an updraft velocity (Braga et al., 2021a; Pöhlker et al., 2021; Reutter et al., 2009). These models simulate the expansion and cooling of air, the resulting changes in relative humidity (RH), or saturation ratio, and the activation followed by condensational growth of cloud droplets. Even though parametrizations based on CCN(S_v) successfully explain the N_d measured at cloud bases, the estimated S_v results from the prescribed updraft velocity of the air parcel and the CCN number concentrations, size, and chemical composition. In this framework, S_v increases with height above the lifting condensation level due to adiabatic cooling of the rising air parcel and further on decreases as the condensational growth of activated CCN depletes water vapor in the saturated parcel (Rogers and YAU, 1989; Squires, 1952).

In this study, we derive S_v at cloud base by describing the ascent of a saturated air parcel as a reversible cloud-adiabatic process. S_v is quantified from the energetic budget of the saturated parcel calculated under the assumption of conserved isobaric enthalpy (Rogers and YAU, 1989). We consider that the atmospheric pressure variability at cloud-base layer is negligible, typically in the order of 10^{-3} (≈ 0.1 - 0.3 %) relative to ambient pressure. The maximum energy available for the conversion of water vapor into liquid water is given by the magnitude of the sensible enthalpy change associated with adiabatic cooling during saturated parcel ascent. This energy is released as latent heat (Q) during condensation of water vapor on CCN and cloud droplets. The resulting energetic balance follows the first law of thermodynamics, such that the latent heat release is partitioned between the change in internal energy of the parcel (ΔU) and the saturation work of water vapor (W_s), i.e., $Q = \Delta U + W_s$. This partition provides an energetic basis to decompose cloud supersaturation into a liquid (S_l) contribution associated with ΔU, and a vapor (S_v) contribution associated with W_s (i.e., $S_l \propto \Delta U/Q$ and $S_v \propto W_s/Q$).

Figure 1 schematizes the energetic closure at cloud base. A saturated parcel at cloud base (T_0, p_0) undergoes a small upward displacement to slightly lower pressure ($p < p_0$), cooling adiabatically to temperature T. Under the assumption of conserved isobaric enthalpy, the parcel is characterized by a constant equivalent temperature (T_e) during the cloud-base ascent. In the absence of condensation and for a small pressure change, the sensible enthalpy change associated with adiabatic cooling is limited by $c_{p,cloud}$ ($T_0 - T$), which represents the upper bound on the parcel's decrease in sensible enthalpy between the two

https://doi.org/10.5194/egusphere-2026-795
Preprint. Discussion started: 17 February 2026

thermodynamic states. Under conserved enthalpy, this change in sensible enthalpy defines the maximum latent heat that would be required for the conversion of water vapor into liquid water, i.e., $Q \approx c_{p,cloud}\,(T_0 - T)$. However, the pressure decrease necessarily implies expansion of the water-vapor component, and a fraction of the latent heat released is expended as saturation work. The term W_s accounts for the energy associated with this vapor expansion as the parcel adjusts to the lower pressure, thereby reducing the energy available to offset the sensible cooling and consequently limiting the conversion of water vapor into liquid water relative to the case in which W_s is neglected.

To apply our method for in situ measurements of cloud properties, we rely on the reversibility of the cloud adiabatic parcel under conserved isobaric enthalpy, in which Q is directly calculated based on measured liquid water content - LWC, T and p at cloud bases, while ΔU and W_s are estimated based on the adiabatic assumptions described. The airborne measurements were conducted over the Amazon Basin at the cloud bases of growing convective cumuli. The data were collected in September 2014 during the ACRIDICON-CHUVA campaign (Wendisch et al., 2016). Clouds were probed under polluted conditions over forested and deforested regions, and under clean marine conditions over the Atlantic Ocean near the Brazilian coast. The $N_d(S_v)$ spectra measured at cloud bases were compared with the CCN(S_v) spectra measured below cloud bases to evaluate the validity of the physical basis for cloud supersaturation estimates.

https://doi.org/10.5194/egusphere-2026-795
Preprint. Discussion started: 17 February 2026

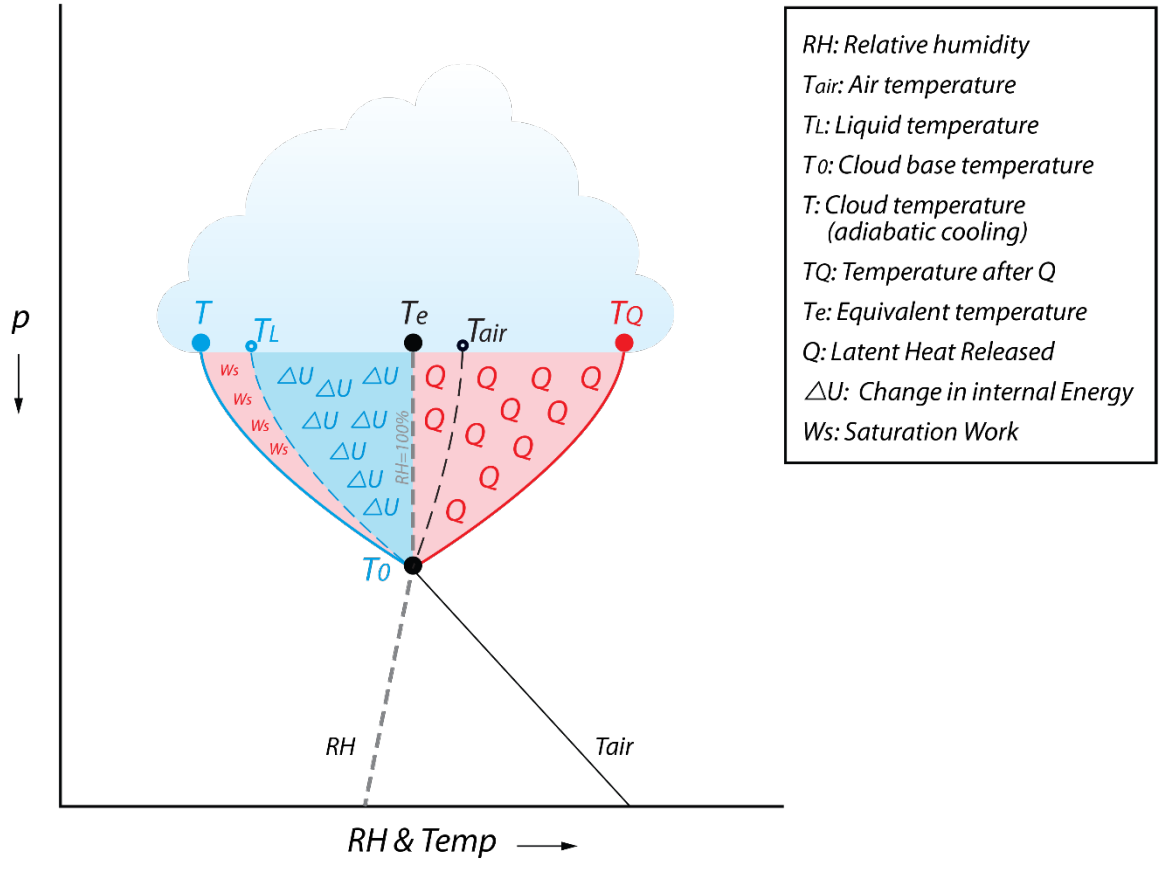

Figure 1. Energy balance of a cloud-adiabatic parcel at cloud base under the assumption of conserved isobaric enthalpy (T_e is constant). Below cloud base, the moist air parcel ascends due to buoyant force, T_{air} decreases with altitude while RH increases up to saturation level of water vapor (RH = 100%) at cloud base (T_0). Above this level, the ascending saturated parcel cools adiabatically as pressure (p) slightly decreases to a given level (T). This process leads to water vapor supersaturation when condensational particle growth is neglected, due to the lower internal energy of the saturated parcel. Under the assumption of conserved isobaric enthalpy, the latent heat released by condensation (Q) is proportional to the cooling rate from T_0 to T. During the condensational growth of CCN particles and droplets, Q is balanced with the decrease in internal energy (ΔU) and saturation work of water vapor (W_s), resulting in a temperature of the liquid parcel (T_L) that is warmer than T. The associated energy balance produces an inversion in the vertical profile of T_{air} where the cloud is formed.

https://doi.org/10.5194/egusphere-2026-795
Preprint. Discussion started: 17 February 2026

2 Methods

To incorporate the thermodynamic constraints of the proposed energy balance at cloud base and calculate the supersaturations at cloud bases, we expanded the classical RH formulation for saturated conditions and derived a new expression for the relative humidity (RH_c). RH_c is calculated from the Clausius-Clapeyron equation for a water vapor-saturated, rising air parcel undergoing expansion (cooling) at temperatures ≥ 0 °C. The degree of cooling (e.g., from T_0 to T shown in Figure 1) determine RH_c and the cloud supersaturation (S_c) at cloud bases. In these conditions, the parcel saturated with water vapor has $RH_c \leq 100\%$; S_c results from vapor excess relative to the initial (warmer) saturation condition (RH_c = 100%), and it is assumed that initially S_c is not diminished by condensation of water vapor on the CCNs or droplets. Under the assumption of conserved isobaric enthalpy, we associate S_c from adiabatic cooling to the latent heat of condensation Q, which is further partitioned into contributions from the liquid phase (S_l) and the vapor phase (S_v). Since S_v is derived from a single temperature gradient, it corresponds to those values of a CCN counter, in which the vapor density results solely from a thermal gradient under saturated conditions (Roberts and Nenes, 2005).

In situ measurements at the cloud bases of growing cumulus clouds were used to validate our theoretical assumptions. The measurements over the Amazon during the ACRIDICON-CHUVA campaign were conducted in clean and polluted conditions across different land cover types (forested, deforested, and urban) and over the Atlantic Ocean. The CCN(S_v) spectra measured just below cloud base prior to cloud base penetrations were used for comparison with the $N_d(S_v)$ spectra calculated at cloud bases during flights in the Central Amazon. The following sections describe the calculations of the thermodynamic, energetic and microphysical properties of clouds, and the data from cloud and meteorological probes and CCN counters used in this study. Table 1 explains the variables described in this section.

2.1 *Description of RH_c and S_c derivation*

The formulation of RH describes the amount of water vapor in the air relative to the amount of water vapor in the air when it is saturated for a given temperature, i.e., the saturation ratio, and is defined as follows:

$$RH = \frac{e(T)}{e_s(T)} \qquad (1)$$

Where $e(T)$ is the water vapor pressure (Pa), $e_s(T)$ is the saturation water vapor pressure (Pa), and T is the air temperature (K or °C) (Bolton, 1980; Rogers and YAU, 1989). The values of e_s can be calculated for a wide range of temperatures (-30 °C ≤ $T_c \leq$ 35 °C) with minor uncertainties (~ 0.1%) as follows:

$$e_s = 611.2 \cdot exp\left(\frac{17.67 \cdot T_c}{T_c + 243.5}\right) \quad [Pa] \quad (2)$$

https://doi.org/10.5194/egusphere-2026-795
Preprint. Discussion started: 17 February 2026

The classical definition of water-vapor supersaturation (S_v) as a function of RH is the following:

$$S_v = \frac{e(T) - e_s(T)}{e_s(T)} = RH - 1 \quad (3)$$

Where RH = 1 (or 100%) is the relative humidity of a saturated parcel. The assumption behind taking RH = 100% as the saturation threshold is that $e_s(T)$ is defined as the equilibrium vapor pressure over a flat surface of pure liquid water. In this condition, evaporation and condensation are balanced. This is based on the Clausius–Clapeyron relation, which describes $e_s(T)$ as the vapor pressure at which liquid water and vapor coexist in thermodynamic equilibrium at temperature T. Thus, S_v is positive when RH > 1 (condensation > evaporation), null at equilibrium state (condensation = evaporation), and negative under subsaturated conditions (condensation < evaporation).

An ascending air parcel in the lower troposphere reaches saturation through a transient non-equilibrium state, where cooling initially exceeds the rate of condensation. This process occurs because decreasing pressure with altitude promotes the expansion of water vapor, which does work and cools adiabatically in the absence of any heat added to the air parcel. When the air parcel reaches saturation of water vapor, latent heat is released as CCN particles activate into cloud droplets and grow by condensation. The relative humidity of a saturated parcel or cloud (RH_c) under expansion is as follows:

$$RH_c = \frac{e_s(T)}{e_s(T_0)} \quad (4)$$

Where $e_s(T_0)$ is the vapor pressure at the reference level, and $e_s(T)$ is the vapor pressure given at a higher level. In this study, the reference level is the cloud base (or the lifting condensation level); thus, at higher levels, the cloud parcel is cooler, leading to $RH_c < 1$.

At the earliest stages of condensational growth, a rising saturated parcel cools by expansion and decreases the internal energy while warming due to latent heat release. When the enthalpy is conserved with height, the equivalent temperature (T_e) is constant, even though the actual temperature varies along the cloud-adiabatic lapse rate. T_e can be written as:

$$T_e = T + \Delta T_Q \quad [K] \quad (5)$$

Where T is the air temperature after adiabatic cooling, and ΔT_Q is the temperature increase that would occur if all water vapor condensed and its latent heat were used to warm the air.

Another important physical property of a saturated parcel is the relationship between $e_s(T)$ and the specific volume of water vapor (α_v), described as follows:

$$e_s(T) = \frac{R_v \cdot T}{\propto_v} \quad [Pa] \quad (6)$$

https://doi.org/10.5194/egusphere-2026-795
Preprint. Discussion started: 17 February 2026

Where R_v is the gas constant for water vapor (461.5 J kg^{-1} K^{-1}). The α_v and the water vapor density ($\rho_v = \alpha_v^{-1}$) are inherently governed by the Clausius–Clapeyron relation through the temperature dependence of $e_s(T)$, where ρ_v defines the mass of water vapor per cubic meter of saturated air.

Equation 6 shows that $e_s(T)$ depends inversely on the α_v. For a saturated parcel expanding and cooling, α_v increases (due to decreasing pressure - p) and hence $e_s(T)$ decreases. The relationship between α_v and p for a saturated parcel can be given by the following equation:

$$\propto_v = \frac{R_v \cdot T \cdot (r_s + R_d/R_v)}{r_s \cdot p} \quad [m^3 kg^{-1}] \quad (7)$$

Where R_d is the gas constant for dry air (287.05 J kg^{-1} K^{-1}), and r_s is the saturation water vapor mixing ratio (kg^{-1}kg^{-1}), which can be calculated as follows:

$$r_s = (R_d/R_v) \cdot \frac{e_s(T)}{p - e_s(T)} \quad [kg^{-1}kg^{-1}] \quad (8)$$

From equations 1, 4, 5, and 6, the RH_c can be described as an isothermal condition in terms of T_e as a function of α_v in different levels near cloud bases as follows:

$$RH_c = \frac{\frac{R_v \cdot T_e}{\alpha_v}}{\frac{R_v \cdot T_e}{\alpha_{v0}}} \quad (9)$$

Where α_{v0} is the specific volume of water vapor at a reference level, and α_v is the specific volume of water vapor after expansion. Expanding Equation 9 from Equation 6, RH_c can be expressed as the following:

$$RH_c = \frac{\propto_{v0}}{\propto_v} = \frac{\rho_v}{\rho_{v0}} = \frac{T_0}{T} \cdot \frac{e_s(T)}{e_s(T_0)} \quad (10)$$

Where T_0 and ρ_{v0} denote the temperature and vapor density of the saturated parcel at the reference (cloud base) state, and T and ρ_v represent the corresponding temperature and vapor density of the parcel after adiabatic expansion. For cloud bases, $T = T_0$ and $RH_c = RH = 1$, and above cloud bases, $RH_c < 1$ since the vapor density is not lost by condensation.

Note that for a saturated parcel, the expansion is governed by temperature through the Clausius–Clapeyron relation, as $e_s(T)$ decreases exponentially with cooling. Therefore, Equation 10 can be expanded based on a first approximation of the Clausius-Clapeyron equation for a constant Latent Heating of Vaporization (L_v), in which the following formulation is valid:

$$\frac{e_s(T)}{e_s(T_0)} = \exp\left[\frac{L_v}{R_v} \cdot \left(\frac{1}{T_0} - \frac{1}{T}\right)\right] \quad (11)$$

L_v depends weakly on temperature change, about 6% for temperatures between -30 °C and 30 °C (Bolton, 1980). In this study, we calculate L_v as a function of temperature (in °C) using the equation below (Bolton, 1980):

https://doi.org/10.5194/egusphere-2026-795
Preprint. Discussion started: 17 February 2026

$$L_v = (2.501 - 0.00237 \cdot T) \cdot 10^6 \quad [J\,kg^{-1}] \quad (12)$$

From Equations 10 and 11, RH_c can be written (in percentage) as follows:

$$RH_c = 100 \cdot \left(\frac{T_0}{T}\right) \cdot exp\left[\frac{L_v}{R_v} \cdot \left(\frac{1}{T_0} - \frac{1}{T}\right)\right] \quad [\%] \quad (13)$$

And from Equation 13, the supersaturation of the cloud (S_c) can be calculated as follows:

$$S_c = 100 - RH_c \quad [\%] \quad (14)$$

Equation 14 describes S_c above cloud base, where RH = 100% is the physical basis condition for saturation. During the cloud parcel ascent, when condensation of CCN and droplets is neglected, RH_c < 100% and S_c is the excess of vapor density resulting from the warmer parcel ascent with a saturation threshold of 100%. Thus, S_c accounts for the vapor-phase (S_v) and liquid-phase (S_l) supersaturation. Note that in Equation 3, S_v is a local relative condition for vapor excess for a cloud parcel saturated at RH =100%, while S_c is a relative condition for liquid and vapor excess in a cloud parcel saturated in RH_c < 100%.

In this study, RH_c and cloud supersaturations (see Section 2.3) are calculated for cloud bases where temperature gradients have typically do not exceed ~1 K. For modelling purposes, the calculation of RH_c and cloud supersaturation may be performed using smaller temperature gradients to reduce thermodynamic uncertainty. Furthermore, the calculation of RH_c must account for the S_v remaining after the first and subsequent time steps of the saturated parcel ascent, as this residual represents excess vapor density that was not converted into liquid water.

2.2 *The Energy Balance in the Cloud Adiabatic Ascent*

Figure 1 described the energy balance of a cloud-adiabatic parcel near cloud base under the assumption of conserved isobaric enthalpy. The energy balance assumptions are detailed in the following steps:

1. Buoyancy-driven ascent and pre-condensation cooling: the saturated parcel rises from cloud base (T_0, p_0) due to a positive buoyancy force generated by its lower density relative to the surrounding air. During this initial upward displacement, no condensation has yet occurred, and the parcel cools adiabatically and retains its initial vapor density (ρ_{v0}) and mixing ratio (r_{s0}). This brief ascent produces a thermodynamic vapor excess, since the ρ_{v0} exceeds the saturation vapor density (ρ_v) at the cooler temperature T.

2. Energetic requirement imposed by conserved isobaric cloud enthalpy: for a reversible cloud-adiabatic parcel the sensible enthalpy resulting from adiabatic cooling from T_0 to T defines the latent-heating requirement that condensation must subsequently supply for the parcel to return to the saturated cloud-adiabatic state. The cloud-enthalpy constraint in terms of the magnitude of energy is calculated as follows:

$$Q = L_v \cdot q_l = \left(c_{p,cloud} \cdot (T_0 - T)\right) = |\Delta U| \quad [J\,kg^{-1}] \quad (15)$$

https://doi.org/10.5194/egusphere-2026-795
Preprint. Discussion started: 17 February 2026

Where q_l is the liquid water mixing ratio (kg^{-1} kg^{-1}), $c_{p,cloud}$ is the specific heat capacity of cloudy air (J kg^{-1} K^{-1}). The q_l and $c_{p,cloud}$ are defined as the following:

$$q_l = LWC/\rho_{air} \quad (16)$$

and,

$$c_{p,cloud} = c_{pd} + c_{pv} \cdot r_s + c_{pl} \cdot q_l \quad (17)$$

Where, ρ_{air} is the dry air density (kg m^{-3}), LWC is the liquid water content (kg m^{-3}), r_s is the saturation water vapor mixing ratio (kg^{-1} kg^{-1}), c_{pd} is the specific heat of dry air at constant pressure (1005 J kg^{-1} K^{-1}), c_{pv} is the specific heat of water vapor at constant pressure (1850 J kg^{-1} K^{-1}), c_{pl} is the specific heat of liquid water at constant pressure (4218 J kg^{-1} K^{-1}). Note that the specific heat of moist air is assumed to be at constant pressure since it varies very weakly (about 2%) between -30 °C and 30 °C (Rogers and YAU, 1989).

3. Condensational growth and the first law of thermodynamic partitioning: as the parcel reaches supersaturation at the cooler level, condensation starts. The latent heat release (Q) is balanced by the decrease in internal energy due to condensation and the mechanical expansion of water vapor, as expressed by the saturation-work term W_s. The first law of thermodynamics, expressed in terms of the magnitudes of the energy components for a reversible saturated parcel, is:

$$Q = |\Delta U_{ws}| + W_s \quad (18)$$

Where, ΔU_{ws} is the change in internal energy, including W_s in the energy balance. The heat added to the system (Q) must satisfy the following balance:

$$|\Delta U_{ws}| = Q - W_s = \left(c_{p,cloud} \cdot (T_0 - T_{ws})\right) \ [J\ kg^{-1}] \quad (19)$$

Where T_{ws} is the effective temperature of the cloud parcel (or T_L shown in Figure 1). For modelling purposes, when LWC is estimated, Q results from the temperature gradient during adiabatic cooling (ΔU) for a given thermodynamic condition, while for airborne measurements, Q is calculated from LWC, p, T and T_0 (estimated). The term W_s can be calculated as a function of r_s and α_v as follows:

$$W_s = \int_{\alpha_{v0}}^{\alpha_v} \frac{R_v \cdot T_{ws} \cdot r_s}{\alpha} \, d\alpha \quad [J\ kg^{-1}] \quad (20)$$

And expanding this equation can be written as follows:

$$W_s = r_s \cdot R_v \cdot T_{ws} \cdot ln\left(\frac{\alpha_v}{\alpha_{v0}}\right) = r_s \cdot R_v \cdot T_{ws} \cdot ln\left(\frac{T_{ws} \cdot e_s(T_0)}{T_0 \cdot e_s(T_{ws})}\right) \quad [J\ kg^{-1}] \quad (21)$$

https://doi.org/10.5194/egusphere-2026-795
Preprint. Discussion started: 17 February 2026

Equation 21 emphasizes that any measurable work done by water vapor during expansion can be interpreted as a quantifiable entropy loss by the saturated parcel. Furthermore, W_s is linearly dependent on T_{ws} and r_s, and is closely associated with RH_c (see Eq. 10).

In the lower troposphere, these microphysical processes occur within a turbulent environment, where expansion, condensation, and latent-heat release can occur almost simultaneously and continuously interact. However, for modeling purposes, this sequence is treated as a stepwise process to isolate the thermodynamic contributions of each term in the energy balance, in which the time scale for buoyant expansion to increase vapor density is faster than the microphysical time scale for condensational growth to remove vapor excess (Korolev and Mazin, 2003).

2.3 *Cloud Supersaturation Partition (Liquid and Vapor phases)*

The energy balance calculated from Eqs. 15 and 19 show that the temperature gradient during the cooling process is different when considering or not W_s. Nevertheless, the total energy Q is conserved. Here, we associate the supersaturation of liquid (S_l) and vapor (S_v) phases with these differences in the temperature gradients. The temperature gradient ($T_0 - T$) is associated with the parcel LWC and Q to S_c (calculated in Section 2.1). S_l and S_v are calculated as a function of the total energy released during the condensational growth given by Q, where ΔU_{ws} and W_s are the energies associated with the liquid and gas phases of S_c as follows:

$$S_l = S_c \cdot \frac{|\Delta U_{ws}|}{Q} \quad [\%] \quad (22)$$

and,

$$S_v = S_c \cdot \frac{|W_s|}{Q} \quad [\%] \quad (23)$$

and,

$$S_c = S_l + S_v \quad [\%] \quad (24)$$

Equations 22-24 describe the relationships between S_c, S_l, and S_v to the energy balance in a saturated parcel in which the isobaric enthalpy is conserved. The fraction of S_l (FS_l) in S_c is associated with the decrease of the internal energy of the saturated parcel (given by equation 22), and the fraction of S_v (FS_v) in S_c is associated with W_s (given by equation 23).

2.4 *Closure analysis from airborne measurements at cloud bases*

The calculations of RH_c and cloud supersaturations (S_c, S_l, and S_v) at cloud bases are performed as a function of the measurements from cloud probes and meteorological sensors on board the HALO aircraft. Table 2 summarizes the general

https://doi.org/10.5194/egusphere-2026-795
Preprint. Discussion started: 17 February 2026

thermodynamic conditions and time intervals of cloud properties measured at cloud bases. In this study, we focus on the initial stage of cloud formation, and thus, cloud passes with a number concentration of droplets (N_d) greater than 20 cm^{-3}, developing in updraft conditions, are considered. This threshold of N_d is used to avoid haze and well-mixed cloud elements in the analysis. Furthermore, cloud passes with measured raindrops are removed from our analysis.

The closure analysis relies on the reversibility of the cloud adiabatic parcel as described in the previous section. The calculations of RH_c, S_c, S_l, and S_v require the information of p, LWC, T, and T_0 near cloud bases. From the airborne data at cloud bases, p, T and LWC are measured. Therefore, we estimate T_0 and T_{0ws} for each cloud pass. Below are the sequential steps used in our analysis:

1. First, T_0 is estimated based on the measured Q (calculated from LWC, T and p) for each cloud pass iteratively using equation 15. RH_c and S_c are calculated from T and estimated T_0 ($T_0 > T$) using equations 13 and 14.
2. The process is repeated, considering Q, calculated in the first step, and W_s in the energy budget (see Eq. 18), which leads to a cooler estimated T_0 (T_{0ws}) than in step 1, where $T_0 > T_{0ws} > T$. From this closure analysis, the values of ΔU_{ws} and W_s are estimated, and S_l and S_v are calculated with equations 22 and 23, respectively.

2.5 *Aircraft Data*

2.5.1 Meteorological measurements

HALO was equipped with a meteorological sensor system (BAsic HALO Measurement And Sensor System– BAHAMAS) located at the nose of the aircraft (Wendisch et al., 2016). The water vapor mixing ratio and derived humidity quantities were measured by the Sophisticated Hygrometer for Atmospheric Research (SHARC). The uncertainties for measurements of air pressure, temperature, relative humidity, mixing ratio, and wind speed are about 3 Pa, 0.5 K, 5 %, 4% and 0.3 m s^{-1}, respectively (Mallaun et al., 2015).

2.5.2 Cloud probe measurements

The measurements of cloud properties over the Amazon Basin were performed by the CCP mounted below the wings of the aircraft (Lance, 2012). CCP combines two detectors, the Cloud Droplet Probe (CDP) and the grayscale Cloud Imaging Probe (CIPgs), which allow the measurement of droplets with a size range of 3-960 µm. In this study, the integrated water content of CDP for bin diameters ranging from 3-50 µm was used to calculate the LWC at warm cloud bases. The measurements were validated by another cloud probe (CAS-DPOL) and a hot wire King probe (Campos Braga et al., 2017). The integrated water content of CIP for bin diameters greater than 50 µm was used to calculate the Rainwater Content (RWC). Only cloud passes without rain droplets (i.e., RWC = 0 g m^{-3}) are used in our analysis.

https://doi.org/10.5194/egusphere-2026-795
Preprint. Discussion started: 17 February 2026

2.5.3 CCN measurements

During the ACRIDICON-CHUVA campaign, two CCN chambers were operating on board the HALO aircraft. Table 3 summarizes the general thermodynamic conditions and the time intervals during which CCN measurements were conducted below cloud base. The CCN(S_v) spectrum of the chambers was compared to the measured N_d and calculated S_v for three flights where N_d(S_v) and CCN(S_v) had the same range of S_v values. The CCN(S_v) spectra were measured below cloud bases prior to cloud base measurements. CCN number concentrations were measured onboard HALO using a two-column CCNC (CCN-200; columns A and B), which is a continuous-flow longitudinal thermal-gradient instrument manufactured by Droplet Measurement Technologies (DMT) (Roberts and Nenes, 2005). The instrument measures CCN number concentration as a function of water vapor supersaturation (S_v) at a frequency resolution of 1 Hz. In the instrument, the sampled aerosol particles are exposed to a set supersaturation and absorb water depending on their size and chemical composition. Particles that grow to droplets larger than 1 µm in diameter are counted as CCN at that S_v. The estimated uncertainty in measurements of CCN number concentration during the ACRIDICON-CHUVA campaign is about 20% (10%) on average for large (small) concentrations (Campos Braga et al., 2017). In addition, the uncertainty in S_v values is 10% on average. Sample air for the aerosol measurements was obtained from two different inlets: (i) the HALO aerosol submicron inlet (HASI) and (ii) the HALO counterflow virtual impactor (HALO-CVI). The CCN-200 provides the possibility to measure from both inlets in parallel or at two different values of S_v.

2.5.4 Airborne meteorological and cloud properties uncertainties

During the ACRIDICON–CHUVA campaign, the resulting uncertainty in the measured N_d and LWC by CCP–CDP with 1 Hz resolution was about 10% (Campos Braga et al., 2017). The uncertainty of rain water content (RWC) measurements was about 30% (Braga et al., 2017, 2021b). RWC uncertainties are less relevant to this study since we are focused on shallow cumulus clouds in the initiation stage of development, which typically have no rain droplets.

Temperature measurements of the considered air parcel at cloud base during individual cloud passes exhibited both cooler and warmer values relative to the surrounding air. This variability arises from the measurement process itself: liquid water impinging on the sensor can induce evaporative cooling, whereas latent heat release from condensational growth and buoyant cloud elements may locally warm the sensor. Nevertheless, these effects are estimated to remain within the nominal uncertainty of the temperature probe (± 0.5 K). Uncertainties in the meteorological measurements from the BAHAMAS system translate into an estimated 4-5% uncertainty in the derived RH_c and S_c. The uncertainties of the energy terms were approximately 10% for Q, 11-15% for ΔU, and 10-11% for W_s. Propagating these errors yields overall uncertainties of ~ 15-17% for S_l and ~ 12% for S_v. The numerical differences between the energy budget calculations performed in the first and second steps described in section 2.4 were negligible (< ~ 0.01% on average).

https://doi.org/10.5194/egusphere-2026-795
Preprint. Discussion started: 17 February 2026

Table 1. List of symbols, variables and physical constants.

Symbol	Description	Units
RH	Relative Humidity	- or %
RH_c	Cloud Relative Humidity	- or %
S	Supersaturation (general, dimensionless)	– or %
S_c	Cloud Supersaturation	%
S_l	Liquid-phase Supersaturation	%
FS_l	Fraction of S_l from S_c	-
S_v	Vapor-phase Supersaturation	%
FS_v	Fraction of S_v from S_c	-
e	Water vapor pressure	Pa
e_s	Saturation vapor pressure	Pa
T	Air temperature	K
T_{ws}	Effective (or Liquid) temperature of the saturated parcel considering W_s	K
T_0	Reference temperature (cloud base)	K
T_{0ws}	Cloud base temperature from closure analysis considering W_s	K
T_e	Equivalent temperature	K
ΔT_Q	Temperature change of saturated parcel due to Q	K
Lv	Latent heat of vaporization	J kg^{-1}
Q	Latent heating released	J kg^{-1}
ΔU	Change in internal energy	J kg^{-1}
ΔU_{ws}	Change in internal energy including W_s	J kg^{-1}
W_s	Saturation work	J kg^{-1}
p	Pressure of the air parcel	Pa
q_l	Liquid water mixing ratio	kg kg^{-1}
r_s	Saturation mixing ratio	kg kg^{-1}
ρ_{air}	Air density	kg m^{-3}
ρ_v	Water vapor density	kg m^{-3}
α_v	Specific volume of water vapor	m^3 kg^{-1}
c_{pd}	Specific heat of dry air (at constant pressure)	J kg^{-1} K^{-1}
c_{pv}	Specific heat of water vapor (at constant pressure)	J kg^{-1} K^{-1}
c_{pl}	Specific heat of liquid water (at constant pressure)	J kg^{-1} K^{-1}

https://doi.org/10.5194/egusphere-2026-795
Preprint. Discussion started: 17 February 2026

$c_{p,cloud}$	Specific heat capacity of cloud air (at constant pressure)	J kg^{-1} K^{-1}
R_d	Gas constant for dry air	J kg^{-1} K^{-1}
R_v	Gas constant for water vapor	J kg^{-1} K^{-1}
N_d	Cloud droplet number concentration	cm^{-3}
r_e	Cloud droplet effective radius	µm
LWC	Liquid Water Content	kg m^{-3} (or g m^{-3})
RWC	Rainwater Content	g m^{-3}

Table 2. Summary of measurement parameters at cloud bases for flights during the ACRIDICON–CHUVA campaign.

Flight	Date in 2014	Initial Time (UTC)	End Time (UTC)	Period of Cloud Measurements (s)	Average Altitude (m)	Average Pressure (hPa)	Average Temperature (°C)
AC07	6-Sep	17:58:00	18:12:50	77	1910	812.3	16.2
AC09	11-Sep	15:41:10	15:53:20	41	1220	878.85	19.5
AC11	16-Sep	17:53:00	18:05:50	33	1896	812.28	16.2
AC14	21-Sep	15:36:40	15:57:30	73	1602	843.4	17.67
AC17a	27-Sep	15:11:40	15:28:40	121	1589	843.28	17.6
AC17b	27-Sep	17:07:00	17:17:00	64	1902	812.3	16.15
AC18	28-Sep	16:46:05	16:55:40	99	1711	834.07	17.18
AC19	20-Sep	17:27:50	17:37:40	163	606.5	942.59	22.26

Table 3. Summary of CCN measurements parameters below cloud bases for flights during the ACRIDICON–CHUVA campaign.

Flight	Date in 2014	Initial Time (UTC)	End Time (UTC)	Period of CCN Measurements (s)	Average Altitude (m)	Average Pressure (hPa)	Average Temperature (°C)
AC11	16-Sep	17:39:10	17:50:00	650	450.93	958.91	28.06
AC14	21-Sep	15:25:00	15:33:20	500	954.9	908.77	22.85
AC17a	27-Sep	14:55:00	15:06:40	700	941.81	908.77	22.87
AC17b	27-Sep	16:52:30	17:01:40	550	1255.4	875.67	21.85

https://doi.org/10.5194/egusphere-2026-795
Preprint. Discussion started: 17 February 2026

3 Results

3.1 *Cloud Supersaturations at cloud bases of Amazonian Clouds*

Cloud supersaturations were calculated from cloud-base measurements over the Amazon Basin across eight flight segments (see Table 2). These observations encompassed diverse environments, including the Central Amazon under the influence of urban pollution, forested regions in the north-northwest, the southern deforestation arc, and the Atlantic Ocean sector (Figure S1 shows the locations of measurements at the cloud bases).

Figure 2 illustrates a case study of the dependence of droplet number concentrations N_d at cloud base on RH, RH_c, cloud supersaturations (S_c, S_l, S_v), and the associated magnitude of energies (Q, ΔU, W_s) derived from measurements collected during Flight AC14. Cloud bases of developing cumuli were measured at about 1600 m altitude and at 17.6 °C. Figure 2a shows that RH (in black) generally increases as a function of N_d even though in most cloud passes RH is smaller than 100%. This variability in RH measurements arises from the characteristics of in situ temperature measurements: liquid water impinging on the sensor can induce evaporative cooling, whereas the latent heat released during particle condensational growth and buoyant air volumes may locally warm the sensor. RH_c (in red) decreases consistently with N_d associated with higher liquid water content LWC. The cloud passes where $RH < RH_c$ indicate that the cloud parcels are likely more affected by entrainment of unsaturated air. Under such conditions, smaller droplets evaporate preferentially due to the inhomogeneous nature of mixing in convective clouds. This selective evaporation reduces the local LWC, and the remaining droplet population is biased toward droplets formed on CCN with higher hygroscopicity, which are more resistant to evaporation. Conversely, for cases in which $RH > RH_c$, cloud elements exhibit stronger buoyancy and more vigorous condensational growth, yielding higher N_d for a given CCN population. These conditions correspond to elevated cloud supersaturation and enhanced LWC.

Figure 2b shows the dependence of N_d on S_v and S_l at cloud base. Both S_l and S_v increase with N_d, although S_v remains nearly one order of magnitude smaller than S_l. Figure 2c presents the energy budget components as a function of S_c, while Figure 2d depicts the cloud supersaturations derived from the measured LWC. These figures show that the total energy (Q) increases strongly with LWC and is dominated by changes in internal energy (ΔU; ~ 89% on average), while the contribution from saturation work (W_s) is comparatively minor.

The fractions of liquid water and water vapor supersaturations (FS_l and FS_v, respectively) as a function of S_c at cloud bases are shown in Figure 3 for the different flight legs measured in the Amazon Basin (see also the closure analysis for all flight segments in Figs. S2-S8). During these flights, FS_l accounted for ~ 88-90% of the S_c, and lower FS_l values were measured for warmer (marine) clouds during flight AC19. FS_v has a strong linear dependence on temperature, since this supersaturation component is associated with the W_s term, which is proportional to the air parcel temperature and saturated mixing ratio (higher at warmer temperatures). These results show that in warmer environments, a larger amount of energy relative to Q is used for the air parcel's expansion, leading to a smaller decrease in the cloud parcel's internal energy and a lower cooling

https://doi.org/10.5194/egusphere-2026-795
Preprint. Discussion started: 17 February 2026

rate. We performed simulations that confirm these findings across a range of thermodynamic conditions (temperature, pressure, and cooling rate) and describe their effects on the energy budget and cloud supersaturation of saturated air parcels in Section S1.

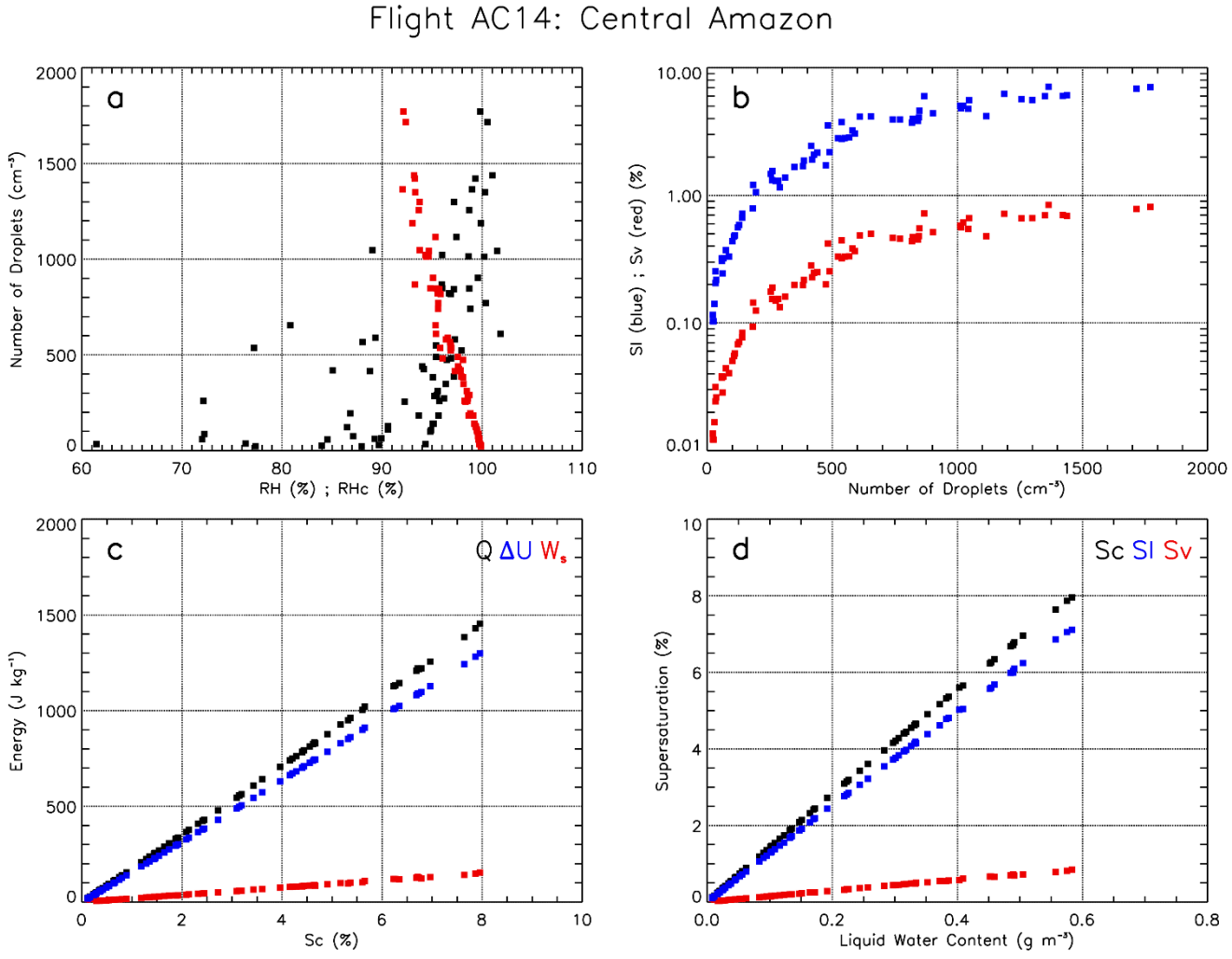

Figure 2. Cloud microphysical and thermodynamic properties measured at cloud bases of growing convective cumuli during Flight AC14. (a) RH versus N_d (black) and RH_c versus N_d (red). Values shown for RH_c do not account for the additional S_v. (b) N_d versus S_l (blue) and N_d versus S_v (red). (c) S_c versus Q, $|\Delta U_{ws}|$ (indicated as ΔU for simplicity), and W_s. (d) LWC versus S_c, S_l, and S_v.

https://doi.org/10.5194/egusphere-2026-795
Preprint. Discussion started: 17 February 2026

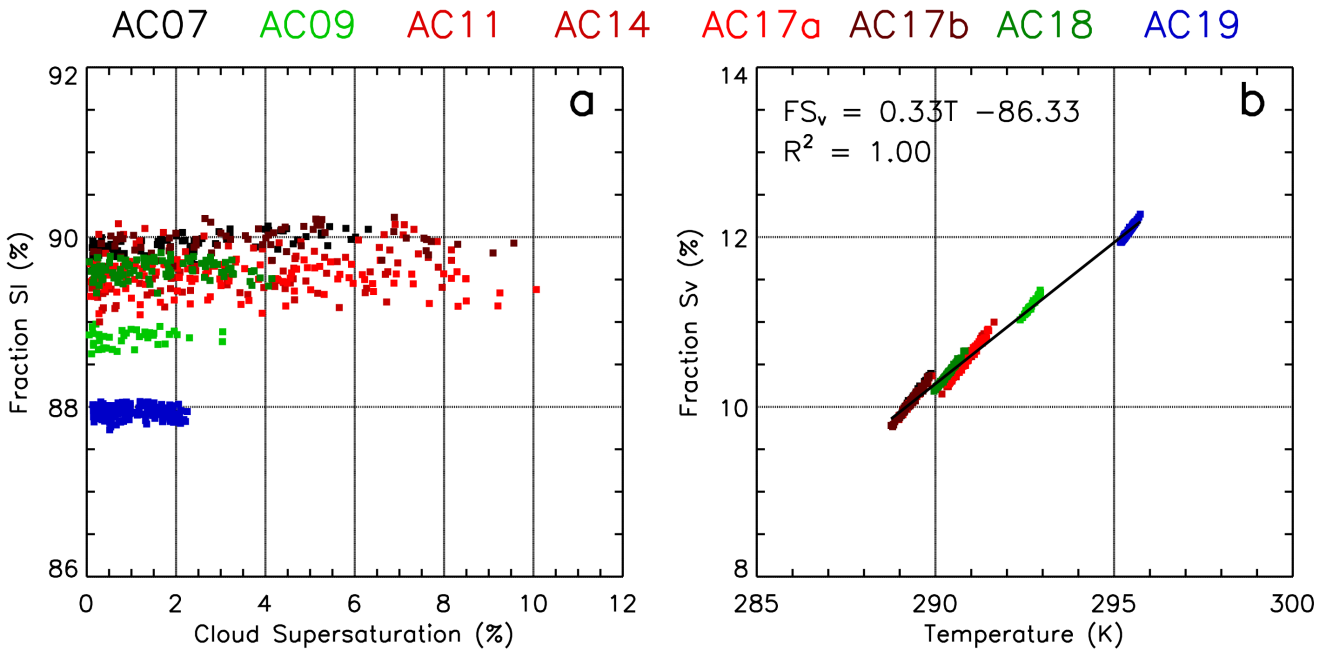

Figure 3. (a) Fraction of liquid-phase supersaturation (S_l) as a function of cloud supersaturation (S_c) for eight cloud segments (AC07, AC09, AC11, AC14, AC17a, AC17b, AC18, AC19). (b) Fraction of water vapor supersaturation (S_v) as a function of cloud temperature.

Figure 4 summarizes the $N_d(S_v)$ spectra at cloud bases for all analyzed flight segments under different atmospheric conditions across the Amazon region. The droplet number spectra $N_d(S_v)$ were derived using power-law fits of the form $N_d = C \cdot S_v^k$, where C is a scaling factor and k is the spectral exponent. Larger k-values indicate stronger sensitivity of droplet activation to S_v, consistent with aerosol-rich conditions (e.g., AC07), whereas smaller k-values (e.g., AC19) reflect more CCN-limited regimes. The high correlation coefficients ($r \geq 0.93$) show robust agreement between observations under different atmospheric conditions. The $N_d(S_v)$ spectra indicate that under marine conditions (flight AC19), the number of droplets expected to activate at cloud base is about 725 cm^{-3} at S_v = 1%. For measurements over forested regions, during flights AC09 and AC18, N_d is roughly twice as large for the same S_v. Even higher values are observed over the Central Amazon and the deforestation arc, where the measured CCN concentrations were more influenced by emissions from urban activities and biomass burning. Clouds forming under CCN-limited regimes were associated with regions of lower buoyant forcing, where lower LWC and updraft speeds were measured (see Figure S9). In contrast, in more polluted environments, buoyant forcing at cloud bases contributes more strongly to droplet formation, as evidenced by higher updraft speeds.

https://doi.org/10.5194/egusphere-2026-795
Preprint. Discussion started: 17 February 2026

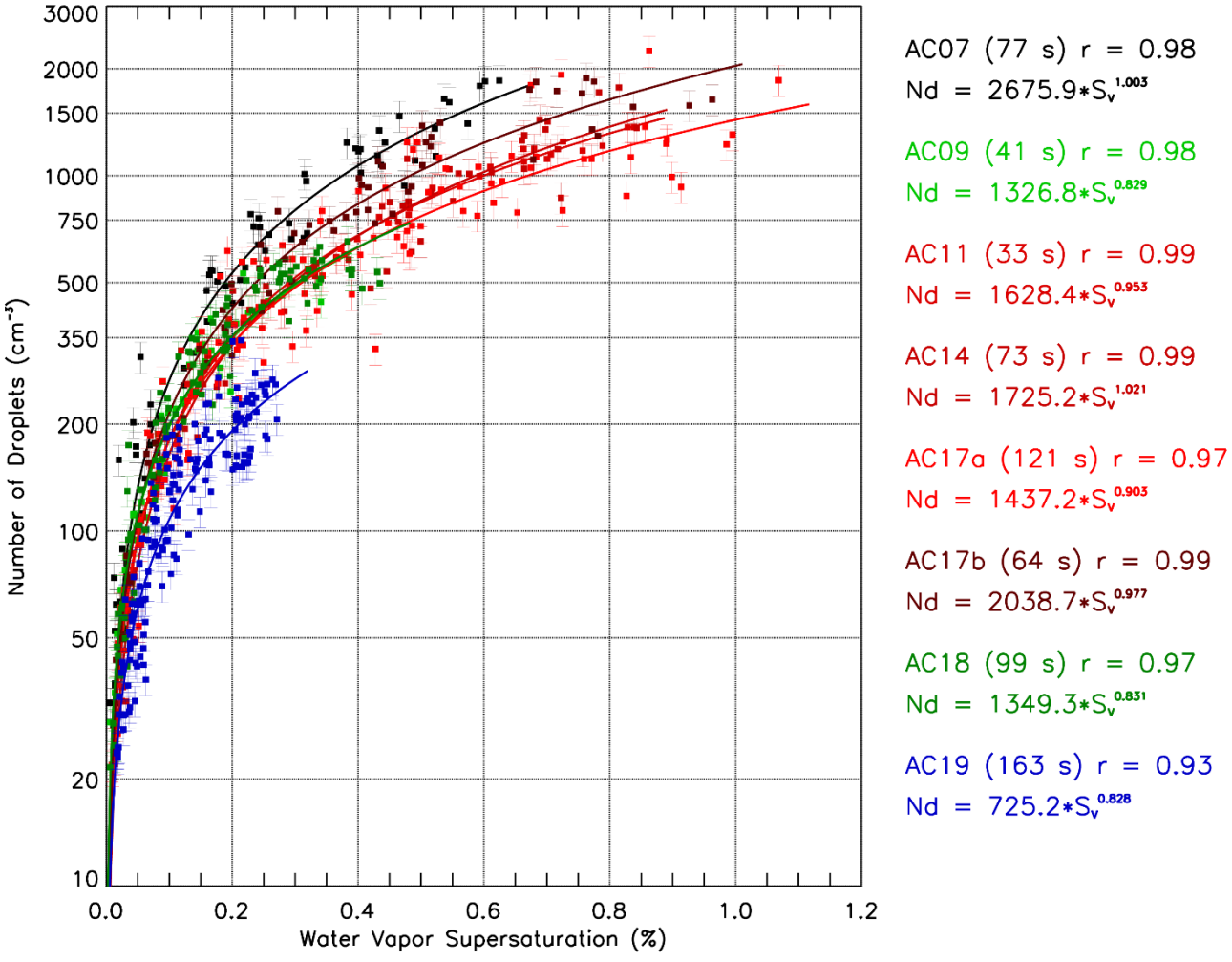

Figure 4. S_v vs. N_d for multiple flight segments (AC07, AC09, AC11, AC14, AC17a, AC17b, AC18, and AC19). Colored markers represent in-situ measurements, while solid curves correspond to power-law fits of the form $N_d = C \cdot S_v^k$. The correlation coefficient (r) of the fit for each flight segment is also indicated. The duration of each analyzed period is given in parentheses. Error bars indicate the uncertainties of N_d (10%).

Similar results were observed for the $N_d(S_l)$ and $N_d(S_c)$ spectra, as shown in Figures S10 and S11, owing to the nearly linear relationship between cloud supersaturations. The $N_d(S_l)$ and $N_d(S_c)$ spectra were derived using similar power-law fits as the water vapor component. Since S_l is associated with the cooling of the cloud parcel, it reflects the relationship between LWC and N_d, where N_d increases steeply for $S_l < 2\%$ before gradually leveling off toward higher values. By incorporating both the liquid (S_l) and vapor (S_v) components of supersaturation, the $N_d(S_c)$ spectra yield correlation coefficients similar to $N_d(S_l)$ and

https://doi.org/10.5194/egusphere-2026-795
Preprint. Discussion started: 17 February 2026

$N_d(S_v)$ spectra. The consistently high correlations across clean and polluted regimes in the Amazon Basin and Atlantic Ocean indicate that N_d is well constrained by S_c, S_l, or S_v.

410

3.2 *Comparison of $N_d(S_v)$ spectra vs. CCN(S_v) spectra in the Central Amazon*

The $N_d(S_v)$ spectra calculated from the energetic budget analysis at cloud bases show a similar magnitude of CCN(S_v) spectra observed below cloud bases in our previous study (Campos Braga et al., 2017). For four flight segments in the Central Amazon, AC11, AC14, AC17a, and AC17b, the CCN(S_v) spectra were measured just below cloud base prior to cloud base
415 measurements with the CCP-CDP probe (see Section 2.5 for airborne measurements description). These measurements allowed comparison of the calculated values of $N_d(S_v)$ measured at cloud bases with CCN(S_v) spectra measured below cloud bases. This analysis is essential to validate the water vapor component of cloud supersaturation, since CCN chamber measurements are not affected by condensational growth processes. For this comparison, the $N_d(S_v)$ spectra were converted to standard temperature and pressure (STP) conditions. During flights AC14 and AC17, the CCN(S_v) measurements were
420 performed about 700 m below cloud base altitude, while during flight AC11, they were performed about 1400 m below cloud base (see Table 3 for additional details).

Figure 5 shows CCN(S_v) spectra for supersaturations ranging from about 0.2% to almost 0.55% during flight AC17, and over a narrower S_v range for flights AC11 and AC14. The figure shows that the $N_d(S_v)$ spectra generally agree within the uncertainty range with the CCN(S_v) activation spectra for all flights. During flight AC11, a relatively higher concentration of
425 particles was measured at $S_v \sim 0.35\%$ by the CCN chamber, while for $S_v > 0.35\%$ CCN(S_v) measurements from both chambers were within the uncertainty range of the $N_d(S_v)$ spectra (~10%). Discrepancies between N_d and CCN concentrations at each S_v primarily reflect differences between the aerosol population sampled several hundred meters below cloud base (about 1400 m) and the fraction of particles subsequently activated at cloud base. Furthermore, CCN counters measure particles that grow to droplets larger than 1 µm in diameter (d), while N_d concentrations are measured for $d > 1.5$
430 µm with CCP-CDP (below this size, the probe has negligible accuracy). Additional deviations may arise from spatial and temporal variations in CCN hygroscopicity between sub-cloud and near-cloud airmasses, which modulate the effective critical S_v measured by CCN counters. In situ temperature measurements during cloud penetrations are also subject to turbulent fluctuations, leading to higher uncertainties in the S_v inferred from cloud measurements.

An improved agreement between CCN(S_v) and $N_d(S_v)$ spectra is shown during the flight legs AC14, AC17a, and AC17b.
435 During these flights, sub-cloud measurements were performed closer to the cloud base (~ 700 m vertical distance below cloud base), which enhances the probability that the measured population of CCN particles was representative of those activated to cloud droplets at cloud bases. During flight AC14, the CCN(S_v) measurements show higher variability, probably affected by the aerosol perturbation from the Manaus urban plume(Campos Braga et al., 2017). The CCN(S_v) spectra from the two flight legs during flight AC17 show the expected trend where the CCN concentrations increase with S_v. In these

https://doi.org/10.5194/egusphere-2026-795
Preprint. Discussion started: 17 February 2026

cases, the overestimation of CCN concentrations appears reliable in comparison to N_d for the same S_v, which seems caused mainly due to differences in the droplet size ranges measured by the CCN counter and cloud probe. Furthermore, values outside the uncertainty range of $N_d(S_v)$ spectra might be influenced by pollution plumes.

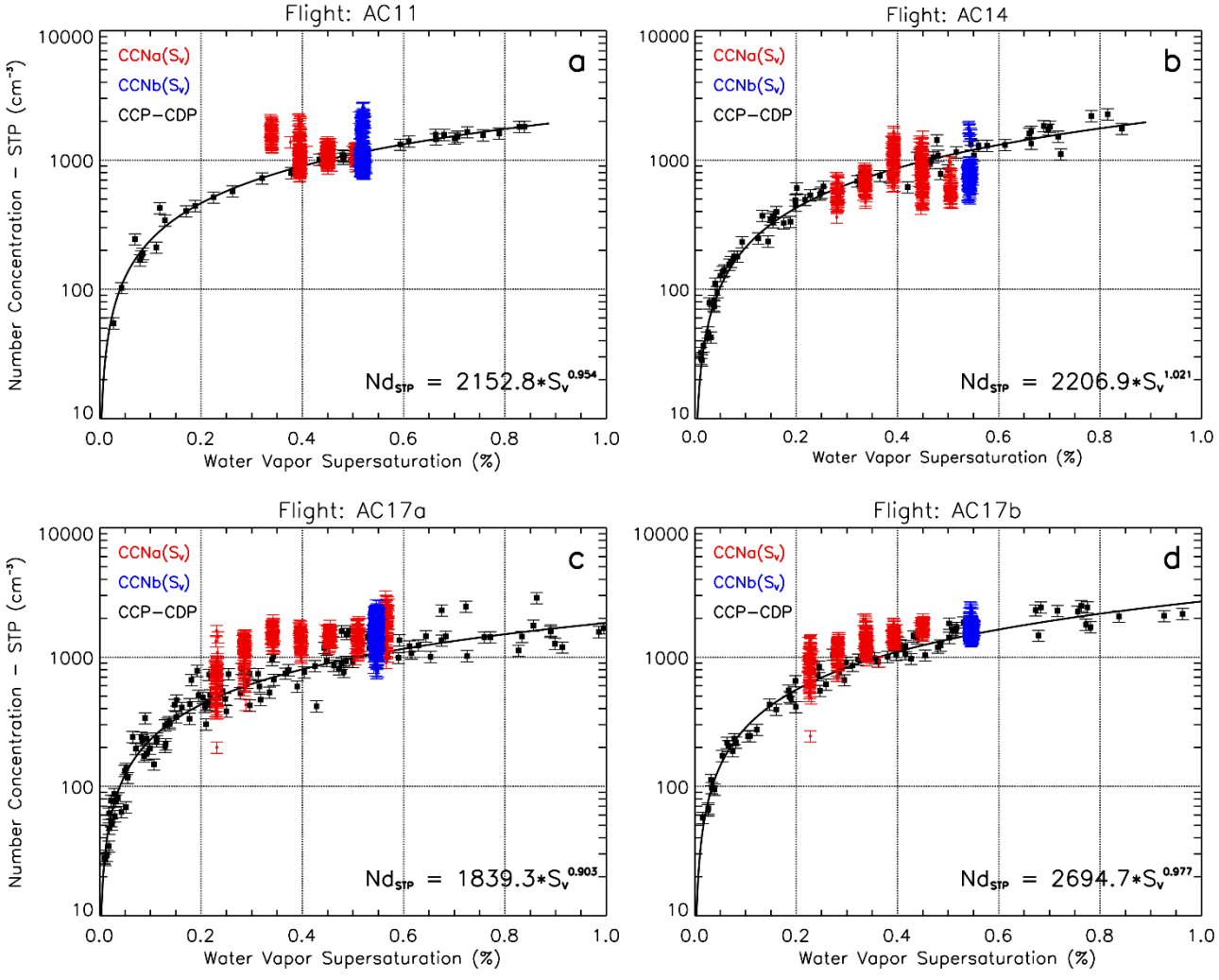

Figure 5. (a) S_v vs. N_d measured at cloud bases (black dots); and S_v vs. CCN concentrations measured below cloud bases (CCNa(S_v) in red and CCNb(S_v) in blue) during Flight AC11. N_d and CCN concentrations are calculated at standard temperature and pressure (STP). Solid curves correspond to power-law fits of the form $N_d = C \cdot S_v^k$. (b), (c), and (d), similar for data from flight legs AC14, AC17a, and AC17b, respectively. Error bars indicate the estimated uncertainties of N_d and CCN(S_v) concentrations (10%).

https://doi.org/10.5194/egusphere-2026-795
Preprint. Discussion started: 17 February 2026

4 Conclusions

The energy budget analysis introduced in this study shows that water vapor supersaturation (S_v) at the bases of warm cumulus clouds can be quantified by treating the ascent of a saturated parcel as a cloud-adiabatic process with conserved isobaric enthalpy. Airborne observations over the Central Amazon reveal that $N_d(S_v)$ spectra at cloud base agree within the uncertainty range of CCN(S_v) spectra measured below cloud base, indicating that the water vapor pressure derived from the thermodynamic equations is physically consistent with that generated in CCN counters. In both cases, the water vapor density results from a thermal gradient under saturated conditions. In CCN counters, S_v is produced within a continuous-flow chamber by imposing controlled temperature gradients (warmer downstream) along wet walls. These gradients promote differential diffusion of water vapor and heat, leading to an enhanced water vapor pressure along the flow axis that exceeds saturation at the local air temperature. The S_v calculated from cloud base measurements is the fraction of the adiabatic cooling energy during the buoyant ascent of the saturated parcel associated with the expansion work of the water vapor in the air parcel (W_s).

The calculated $N_d(S_v)$ spectra at cloud bases in different thermodynamic and aerosol conditions over the Amazon Basin and Atlantic Ocean have shown a typical variability expected by CCN(S_v) spectra measured in clean and polluted conditions (Khain and Pinsky, 2018). However, the methodology relies on several idealized assumptions - thermodynamic reversibility, negligible entrainment (adiabaticity), and accurate in situ microphysical and thermodynamic measurements - that may not fully capture the complexity of heterogeneous and highly turbulent cloud bases. Despite these limitations, the suggested methodology adds new insights for the modelling of cloud base supersaturation and energetics, offering a physically consistent constraint on droplet activation and condensational growth (Khain et al., 2015; Khain and Pinsky, 2018; Korolev and Mazin, 2003; Pinsky et al., 2012; Prabhakaran et al., 2020). It allows estimating N_d as a function of cloud supersaturation (S_c, S_l, and S_v) using in situ measurements of cloud microphysical properties. Under the assumption of conserved isobaric enthalpy at cloud base, the production of supersaturation and the resulting microphysical properties can be inferred from the vertical evolution of a saturated parcel following the cloud-adiabatic lapse rate (~ 3-8 K km^{-1}) relative to the dry adiabatic ascent (~ 9.8 K km^{-1}). Our results suggest that the adiabatic LWC calculated by parcel models overestimates the amount of water vapor that can condense into liquid water since they neglect the energetic cost of vapor expansion (W_s) during the ascent of the saturated parcel. The practical consequence for the energy budget is an overestimation of the latent heat released during condensational growth of CCN and cloud droplets, which in turn leads to an overestimation of the cloud parcel buoyancy and associated updraft speeds.

Future studies applying energetic budget analyses to in situ measurements can be extended to calculate cloud supersaturation at cloud bases in other regions of the globe with different aerosol and thermodynamic conditions. The method described in this manuscript is especially relevant when CCN(S_v) measurements are unavailable. Furthermore, the vertical profiles of microphysical properties within adiabatic cloud parcels should be examined in the context of the energetic budget to infer supersaturation at cloud bases and above, including the ice and mixed-phase regimes. Such extensions will enable a more

https://doi.org/10.5194/egusphere-2026-795
Preprint. Discussion started: 17 February 2026

comprehensive quantification of the coupled microphysical-energetic responses of clouds under diverse atmospheric conditions, encompassing aerosol-cloud interactions, droplet condensational growth and evaporation, and ice-phase processes.

Data availability

The data used in this study can be found at https://halo-db.pa.op.dlr.de/mission/5.

Author contributions

Conceptualization: RCB.
Methodology: RCB.
Investigation: RCB.
Visualization: RCB.
Supervision: DH.
Writing—original draft: RCB, DH.
Writing—review & editing: RCB, DH, MW and RA.

Competing interests

The authors declare they have no competing interests.

https://doi.org/10.5194/egusphere-2026-795
Preprint. Discussion started: 17 February 2026

Acknowledgements

We thank the Reef Restoration and Adaptation Program (RRAP) and Southern Cross University.

Financial support

This work was funded by the The Reef Restoration and Adaptation Program a partnership between the Australian Government's Reef Trust and the Great Barrier Reef Foundation.

References

Bolton, D.: The computation of equivalent potential temperature., Mon. Weather Rev., 108, https://doi.org/10.1175/1520-0493(1980)108<1046:TCOEPT>2.0.CO;2, 1980.

Braga, R. C., Rosenfeld, D., Weigel, R., Jurkat, T., Andreae, M. O., Wendisch, M., Pöschl, U., Voigt, C., Mahnke, C., Borrmann, S., Albrecht, R. I., Molleker, S., Vila, D. A., Machado, L. A. T., and Grulich, L.: Further evidence for CCN aerosol concentrations determining the height of warm rain and ice initiation in convective clouds over the Amazon basin, Atmos. Chem. Phys., 17, 14433–14456, https://doi.org/10.5194/acp-17-14433-2017, 2017.

Braga, R. C., Ervens, B., Rosenfeld, D., Andreae, M. O., Förster, J.-D., Fütterer, D., Hernández Pardo, L., Holanda, B. A., Jurkat-Witschas, T., Krüger, O. O., Lauer, O., Machado, L. A. T., Pöhlker, C., Sauer, D., Voigt, C., Walser, A., Wendisch, M., Pöschl, U., and Pöhlker, M. L.: Cloud droplet formation at the base of tropical convective clouds: closure between modeling and measurement results of ACRIDICON–CHUVA, Atmos. Chem. Phys., 21, 17513–17528, https://doi.org/10.5194/acp-21-17513-2021, 2021a.

Braga, R. C., Rosenfeld, D., Krüger, O. O., Ervens, B., Holanda, B. A., Wendisch, M., Krisna, T., Pöschl, U., Andreae, M. O., Voigt, C., and Pöhlker, M. L.: Linear relationship between effective radius and precipitation water content near the top of convective clouds: measurement results from ACRIDICON–CHUVA campaign, Atmos. Chem. Phys., 21, 14079–14088, https://doi.org/10.5194/acp-21-14079-2021, 2021b.

Campos Braga, R., Rosenfeld, D., Weigel, R., Jurkat, T., Andreae, M. O., Wendisch, M., Pöhlker, M. L., Klimach, T., Pöschl, U., Pöhlker, C., Voigt, C., Mahnke, C., Borrmann, S., Albrecht, R. I., Molleker, S., Vila, D. A., Machado, L. A. T., and Artaxo, P.: Comparing parameterized versus measured microphysical properties of tropical convective cloud bases during the ACRIDICON-CHUVA campaign, Atmos. Chem. Phys., 17, 7365–7386, https://doi.org/10.5194/acp-17-7365-2017, 2017.

Ervens, B., Cubison, M. J., Andrews, E., Feingold, G., Ogren, J. A., Jimenez, J. L., Quinn, P. K., Bates, T. S., Wang, J., Zhang, Q., Coe, H., Flynn, M., and Allan, J. D.: CCN predictions using simplified assumptions of organic aerosol composition and mixing state: A synthesis from six different locations, Atmos. Chem. Phys., 10, 4795–4807, https://doi.org/10.5194/acp-10-4795-2010, 2010.

https://doi.org/10.5194/egusphere-2026-795
Preprint. Discussion started: 17 February 2026

Khain, A. P. and Pinsky, M.: Physical Processes in Clouds and Cloud Modeling, https://doi.org/10.1017/9781139049481, 2018.

Khain, A. P., Beheng, K. D., Heymsfield, A., Korolev, A., Krichak, S. O., Levin, Z., Pinsky, M., Phillips, V., Prabhakaran, T., Teller, A., Van Den Heever, S. C., and Yano, J. I.: Representation of microphysical processes in cloud-resolving models: Spectral (bin) microphysics versus bulk parameterization, https://doi.org/10.1002/2014RG000468, 2015.

Köhler, H.: The nucleus in and the growth of hygroscopic droplets, Transactions of the Faraday Society, 32, 1152–1161, 1936.

Korolev, A. V. and Mazin, I. P.: Supersaturation of Water Vapor in Clouds, J. Atmos. Sci., 60, 2957–2974, https://doi.org/10.1175/1520-0469(2003)060<2957:SOWVIC>2.0.CO;2, 2003.

Lance, S.: Coincidence errors in a cloud droplet probe (CDP) and a cloud and aerosol spectrometer (CAS), and the improved performance of a modified CDP, J. Atmos. Ocean. Technol., 29, 1532–1541, https://doi.org/10.1175/JTECH-D-11-00208.1, 2012.

Mallaun, C., Giez, A., and Baumann, R.: Calibration of 3-D wind measurements on a single-engine research aircraft, Atmos. Meas. Tech., 8, 3177–3196, https://doi.org/10.5194/amt-8-3177-2015, 2015.

[Masson-Delmotte, V., Zhai, P., Pirani, A., Connors, S. L., Péan, C., Berger, S., Caud, N., Chen, Y., Goldfarb, L., Gomis, M. I., Huang, M., Leitzell, K., Lonnoy, E., Matthews, J. B. R., Maycock, T. K., Waterfield, T., Yelekçi, O., Yu, R., Zhou, B., and (eds.): IPCC, 2021: Climate Change 2021: The Physical Science Basis, Cambridge University Press. In Press., 2021.

Pinsky, M., Khain, A., Mazin, I., and Korolev, A.: Analytical estimation of droplet concentration at cloud base, Journal of Geophysical Research Atmospheres, 117, 1–14, https://doi.org/10.1029/2012JD017753, 2012.

Pöhlker, M. L., Zhang, M., Campos Braga, R., Krüger, O. O., Pöschl, U., and Ervens, B.: Aitken mode particles as CCN in aerosol- And updraft-sensitive regimes of cloud droplet formation, Atmos. Chem. Phys., 21, https://doi.org/10.5194/acp-21-11723-2021, 2021.

Prabhakaran, P., Shawon, A. S. M., Kinney, G., Thomas, S., Cantrell, W., and Shaw, R. A.: The role of turbulent fluctuations in aerosol activation and cloud formation, Proc. Natl. Acad. Sci. U. S. A., 117, https://doi.org/10.1073/pnas.2006426117, 2020.

Reutter, P., Su, H., Trentmann, J., Simmel, M., Rose, D., Gunthe, S. S., Wernli, H., Andreae, M. O., and Pöschl, U.: Aerosol- and updraft-limited regimes of cloud droplet formation: influence of particle number, size and hygroscopicity on the activation of cloud condensation nuclei (CCN), Atmos. Chem. Phys., 9, 7067–7080, https://doi.org/10.5194/acp-9-7067-2009, 2009.

Rissler, J., Swietlicki, E., Zhou, J., Roberts, G., Andreae, M. O., Gatti, L. V., and Artaxo, P.: Physical properties of the sub-micrometer aerosol over the Amazon rain forest during the wet-to-dry season transition – comparison of modeled and measured CCN concentrations, Atmospheric Chemistry and Physics Discussions, 4, 3159–3225, https://doi.org/10.5194/acpd-4-3159-2004, 2004.

Roberts, G. C. and Nenes, a.: A Continuous-Flow Streamwise Thermal-Gradient CCN Chamber for Atmospheric Measurements, Aerosol Science and Technology, 39, 206–221, https://doi.org/10.1080/027868290913988, 2005.

Rogers, R. R. and YAU, M. K.: A short course of cloud physics, Third edit., Library of Congress, Oxford, UK, 1989.

https://doi.org/10.5194/egusphere-2026-795
Preprint. Discussion started: 17 February 2026

Squires, P.: The growth of cloud drops by condensation. I. General characteristics, Aust. J. Chem., 5, https://doi.org/10.1071/CH9520059, 1952.

Wang, J., Lee, Y. N., Daum, P. H., Jayne, J., and Alexander, M. L.: Effects of aerosol organics on cloud condensation nucleus (CCN) concentration and first indirect aerosol effect, Atmos. Chem. Phys., 8, 6325–6339, https://doi.org/10.5194/acp-8-6325-2008, 2008.

Wendisch, M., Pöschl, U., Andreae, M. O., Machado, L. A. T., Albrecht, R., Schlager, H., Rosenfeld, D., Martin, S. T., Abdelmonem, A., Afchine, A., Araùjo, A., Artaxo, P., Aufmhoff, H., Barbosa, H. M. J., Borrmann, S., Braga, R., Buchholz, B., Cecchini, M. A., Costa, A., Curtius, J., Dollner, M., Dorf, M., Dreiling, V., Ebert, V., Ehrlich, A., Ewald, F., Fisch, G., Fix, A., Frank, F., Fütterer, D., Heckl, C., Heidelberg, F., Hüneke, T., Jäkel, E., Järvinen, E., Jurkat, T., Kanter, S., Kästner, U., Kenntner, M., Kesselmeier, J., Klimach, T., Knecht, M., Kohl, R., Kölling, T., Krämer, M., Krüger, M., Krisna, T. C., Lavric, J. V., Longo, K., Mahnke, C., Manzi, A. O., Mayer, B., Mertes, S., Minikin, A., Molleker, S., Münch, S., Nillius, B., Pfeilsticker, K., Pöhlker, C., Roiger, A., Rose, D., Rosenow, D., Sauer, D., Schnaiter, M., Schneider, J., Schulz, C., de Souza, R. A. F., Spanu, A., Stock, P., Vila, D., Voigt, C., Walser, A., Walter, D., Weigel, R., Weinzierl, B., Werner, F., Yamasoe, M. A., Ziereis, H., Zinner, T., and Zöger, M.: The ACRIDICON-CHUVA campaign: Studying tropical deep convective clouds and precipitation over Amazonia using the new German research aircraft HALO, Bull. Am. Meteorol. Soc., 160128144638003, https://doi.org/10.1175/BAMS-D-14-00255.1, 2016.